

Transient Approach to Model Operating Point Dependent Losses in Saturated Induction Machines

Georg von Pfingsten, Simon Steentjes, and Kay Hameyer

Abstract -- In this paper, the global operating point dependent losses of induction machines are studied utilizing a local transient loss formulation. After calculating the local loss distribution, the losses are integrated in space and averaged in time to get the average global losses. The main loss components Ohmic losses, iron losses and friction losses are considered. The Ohmic losses in stator and rotor are dependent on current values and the time- and local-waveform due to current displacement. The iron losses are highly dependent on flux density, base frequency, and harmonic distortion of the flux density. The level of flux, the machine is operated at, depends on the operation mode of the inverter. Hence for precise loss modeling of inverter driven induction machines at the machine design stage, time and spatial distribution of flux density and the influence of choosing the best operating point is included.

Index Terms -- Induction Machines, Induction Motors, Iron Loss Modelling, Loss Minimization, Loss Modelling, Magnetic Losses, Ohmic Losses

I. INTRODUCTION

In this paper, the iron losses of a four pole ($2p = 4$) squirrel cage induction machine (SCIM) for an electric vehicle traction application are exemplarily studied through measurements and finite element (FE) simulations. In the application the machine is driven by a MOSFET inverter with a nominal DC-link voltage of 130 V. The machine can deliver a short term maximum power of 37 kW and has a maximum operating speed of $n_{\max} = 8000$ 1/min. The S2-30 min power is 22 kW. In the application, the machine is cooled by the air flow while driving. On the test bench, the machine is cooled by a ventilator to prevent overheating. The stator has $N_1 = 36$ slots, which is equal to a number of slots per pole and phase of $q_1 = 3$. The rotor has $N_2 = 28$ bars/slots. The active length of the machine is $l_{Fe} = 200$ mm. The squirrel cage is made of aluminum in a die casting process.

Several papers have been published in the past decades on the field of loss minimization of induction machines. For effective loss minimization, an accurate loss model of the machine is necessary. In most papers, the machine and loss model parameters are identified from test bench measurements of existing machines [1] – [4]. In [5] a loss minimization is performed on system level employing a fundamental wave machine model considering saturation through limiting the maximum rotor flux linkage. In [6] a fundamental wave machine model considering ferromagnetic saturation through look-up-tables is used. In [6], the iron

losses are modeled using a fundamental wave model. In [7] a dynamic loss model is applied to FE simulations of a PMSM wind power generator. [7,8] show that the iron losses are underestimated if only the fundamental field-wave is considered. This effect is of particular importance when the additional losses resulting from the higher harmonics and minor loops are considered. In [8] a loss minimization is performed for a synchronous machine. In contrast, this paper utilizes a time-domain iron loss model which is parameterized by standardized measurements on ring cores according to the international IEC standard. Therewith, an *a-priori* estimation of loss minimized operating points in induction machines is possible avoiding tedious frequency-domain simulations and extensive test bench measurements of existing machines.

The paper is structured as follows: First, the simulation of the machines operating points is discussed. Secondly the modeling of the operating points from FE simulation is addressed. In the next step, the dynamic iron loss model is described. Subsequent, the scaling of the modeled iron losses from one simulated fundamental frequency to another fundamental frequency is discussed. From the scaling scheme the iron losses are modeled versus the entire torque speed operating map. Finally, the modeled machine operating points and losses are compared to machine measurements. The paper ends with a discussion of the results and conclusions.

II. MACHINE SIMULATION SCHEME

Since the machine is operated as a traction drive for automotive application, the machine characteristic behavior in the entire operating range in terms of torque and speed is of interest. Therefore the losses are given for the torque-speed operating map. Fig. 1 illustrates the structure of the simulation.

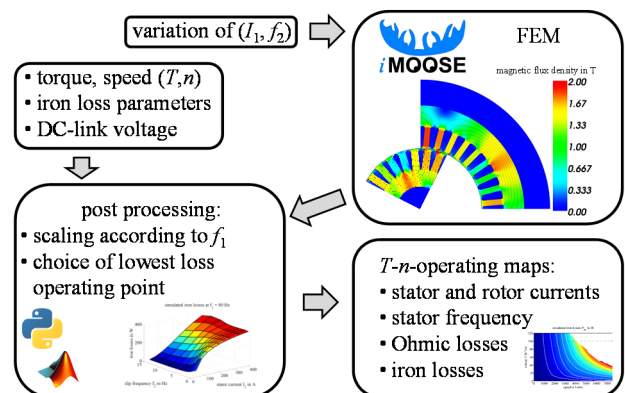


Fig. 1. Machine simulation scheme.

G. von Pfingsten, S. Steentjes, and K. Hameyer are with the Institute of Electrical Machines of RWTH Aachen University, Schinkelstr. 4, 52062 Aachen, Germany (e-mail: georg.vonpfingsten@iem.rwth-aachen.de).

A. Torque speed operating points (measurements)

Induction machines for traction applications are operated at different values of magnetic flux, depending on requested torque and speed.

The fundamental wave T-equivalent-circuit (Fig. 2) illustrates the allocation of the given stator current I_1 into magnetizing current I_μ and rotor current I_2' . Relevant for the allocation of the stator current are the two parallel branches $j\omega_1 L_{1h}$ and $j\omega_1 L'_{2,\sigma} + R'_2 \cdot \omega_1 / 2\pi f_2$. The reactances and the rotor resistance in these branches are proportional to ω_1 . The allocation of the stator current I_1 into magnetizing current I_μ and rotor current I_2' is therefore independent of ω_1 , i.e. of f_1 .

The saturation of the main inductance L_{1h} has to be considered in highly utilized traction drives. Saturation of L_{1h} occurs at high values of I_μ , which is reached at high values of I_1 and low values of rotor frequency f_2 . Hence, the allocation of I_1 into I_μ and I_2' is dependent on the amplitude of I_1 and the rotor frequency f_2 .

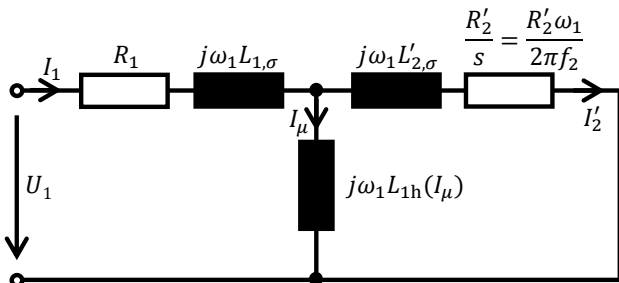


Fig. 2. Fundamental wave T-equivalent-circuit of the SCIM.

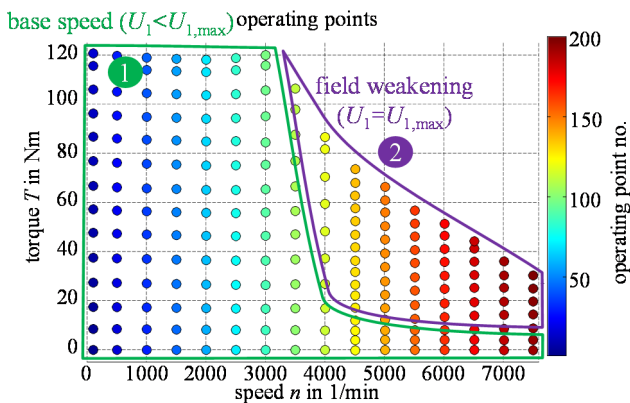


Fig. 3. Measured operating points of the machine in the torque-speed plane.

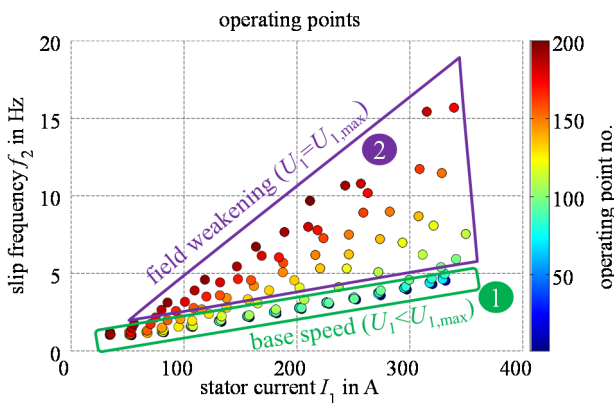


Fig. 4. Measured operating points of the machine in the stator current-slip frequency plane.

Therefore, the operating points (T, n) of the induction machine can be mapped in the stator current – slip frequency plane (I_1 - f_2 -plane). This mapping of measured machine operating points in terms of torque T and speed n (Fig. 3) to the I_1 - f_2 -plane is shown in Fig. 4. The colors of the operating points correspond to their numbering from 1 to 200. Since the same operating points are shown in Fig. 3 and Fig. 4, the operating point numbers, i.e., color of the operating point, are associated. It is apparent, that the base speed ($U_1 < U_{1,max}$) operating points are located in a small section of the I_1 - f_2 -plane with $f_2 < 5$ Hz. The operating points at the voltage limit ($U_1 = U_{1,max}$) are located at higher slip frequency values.

Since the machine operating points are covered on the I_1 - f_2 -plane, the operating points (T, n) of the machine can be simulated rasterizing an area of a reasonable number of combinations of I_1 and f_2 .

In the machine measurements, the total harmonic distortion of the stator current THD_{I1} was measured. In most of the operating points the value of THD_{I1} is between 1 % and 2 %. Except for the no-load operating points ($I_1 = 0$, $T \approx 0$), in all operating points the value of THD_{I1} is less than 5 %. Therefore, the stator current can be assumed to be sinusoidal. The influence of PWM supply on the losses in the machine was determined by measuring the input power with, and without low-pass filtering voltage and current. The error made when filtering the PWM was measured to be less than 20 W. Therefore, harmonics in the stator currents by inverter switching or from the machines are neglected when modelling the Ohmic losses in the stator. Hence the stator Ohmic losses $P_{Cu,1}$ can be easily calculated using the stator Ohmic resistance R_1 and the effective current I_1 according to (1).

$$P_{Cu,1} = 3 \cdot I_1^2 \cdot R_1 \quad (1)$$

B. Torque speed operating points from FE Simulations

Nonlinear transient FE formulations with single valued magnetization curves are used to calculate the local flux density values of the magnetic circuit. The stator current is the only excitation defined in the model. The rotor position and therefore speed n is used to update the rotational boundaries in the air gap for every simulation step. Hence, the stator current (amplitude I_1 and frequency f_1) as well as the slip frequency $f_2 = f_1 - np$ are used to define the operating point in the FE model.

100 combinations of I_1 and f_2 are simulated in order to cover the entire operating range of the machine. A sinusoidal stator current density (and therefore sinusoidal current I_1) is used as excitation for the simulation model. The amplitude of the current density impressed to the stator slot area is varied in 10 steps from 1 to 10 A/mm², which is equal to an effective current of 40 A to 404 A. The slip frequency is varied in 10 steps from 0 to 15 Hz. The region with I_1 less than 189 A and f_2 less than 8 Hz is divided into a smaller grid, since most measured operating points are in this range of I_1 and f_2 . Hence the 100 simulated operating points cover the measured operating points (Fig. 4) in the I_1 - f_2 -plane.

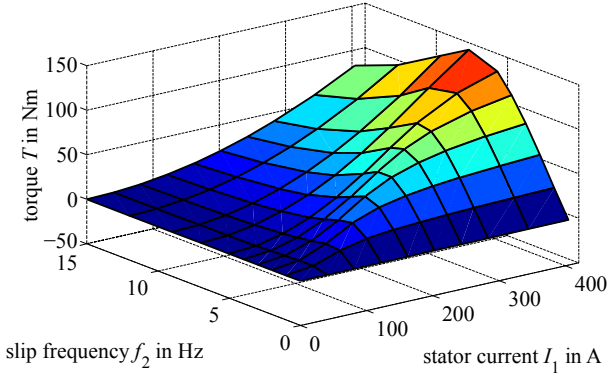


Fig. 5. Simulated torque of the machine (from FE simulations).

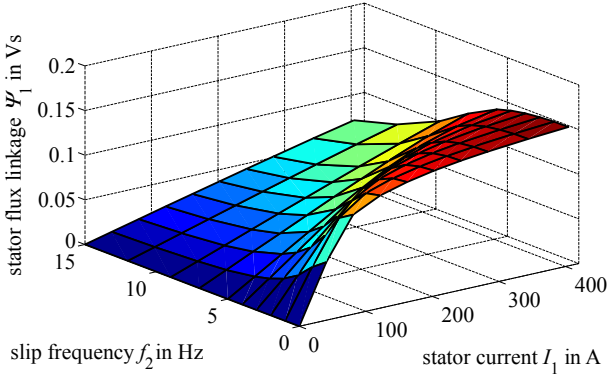


Fig. 6. Simulated stator flux linkage of the machine (from FE simulations).

Fig. 5 and Fig. 6 show the simulation results in terms of torque T and stator flux linkage Ψ_1 in the I_1 - f_2 -plane. It is apparent that the stator flux linkage Ψ_1 is subject to saturation at high stator currents and low slip frequency.

Fig. 7 shows the simulated values of torque and stator flux linkage as projected views. The current densities in the rotor bars are calculated with the help of the FE simulations. Using the current density values $J_{EL,i}$ in every element i with the area $A_{EL,i}$, the rotor Ohmic losses $p_{Cu,2}$ are calculated in every time step t as sum over all elements (2). Thereby, increased rotor Ohmic losses from local current distribution in the rotor bars, i.e. proximity effect, is included. From the rotor Ohmic losses in every simulation step, the average rotor Ohmic losses $P_{Cu,2}$ are calculated (3).

$$p_{Cu,2}(t) = \sum_i \frac{1}{\sigma} J_{EL,i}^2(t) \cdot A_{EL,i} \cdot l_{Fe} \quad (2)$$

$$P_{Cu,2} = \frac{1}{T} \sum_{t=t_0}^{t_0+T} p_{Cu,2}(t) \quad (3)$$

Adding Ohmic losses in stator and rotor, the overall Ohmic losses P_{Cu} are calculated (4). The simulated sum of the Ohmic losses P_{Cu} and the torque T is shown in Fig. 8 across the I_1 - f_2 -plane.

$$P_{Cu} = P_{Cu,1} + P_{Cu,2} \quad (4)$$

The operating points (I_1, f_2) of the machine are determined using the simulation results shown in Fig. 7 and Fig. 8. For every desired torque and speed combination (T_{req}, n_{req}) , the (I_1, f_2) operating point with the highest efficiency (lowest

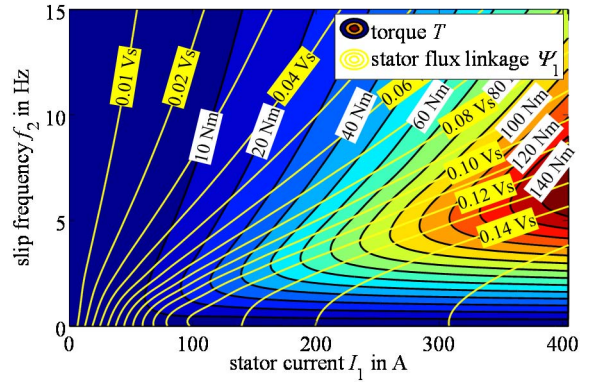


Fig. 7. Simulated torque and stator flux linkage of the machine (FE simulations).

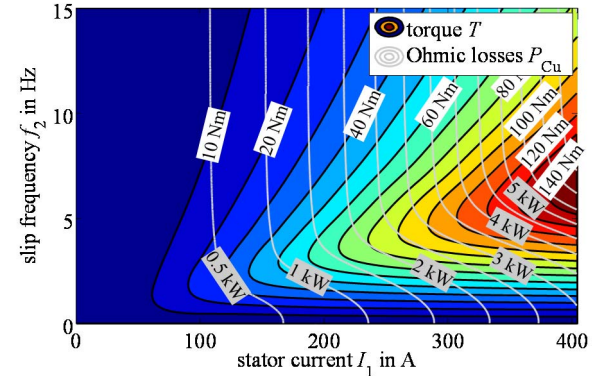


Fig. 8. Simulated torque and Ohmic P_{Cu} losses of the machine (FE simulations).

losses) is sought according to (5). If this (I_1, f_2) combination violates the voltage limit of the inverter, an operating point with less stator flux linkage is chosen. If no point exists, that meets the required torque at the maximum feasible stator flux linkage, the torque-speed combination is found to be not obtainable subject to the given boundaries. Hence, field weakening, i.e. operation at the inverters voltage limit, is regarded in the simulation scheme.

$$\min_{I_1, f_2} P_{Cu}(I_1, f_2) \quad (5)$$

$$\text{s.t. } T(I_1, f_2) = T_{req},$$

$$f_1 = f_2 + n_{req} \cdot p,$$

$$U_1(I_1, f_1) \leq U_{max}$$

The resulting operating points (I_1, f_2) are compared to machine measurements over torque and speed in section E (Fig. 17 and 18).

C. Iron loss modelling from local and temporal magnetic flux density distribution

The maximum fundamental operating frequency of the stator current is 282 Hz. The maximum rotating speed is $n = 8000 \text{ min}^{-1}$. This high frequency and speed lead to significant influence of flux pulsations in the teeth of the machine up to frequencies of multiple kHz. Since the fundamental frequency of the rotor current f_2 is between 0 and 16 Hz (Fig. 4), a wide spread of the magnetizing frequencies

in the rotor and stator soft magnetic material is apparent. When using time harmonic formulations to model the iron losses, a minimal period of $T_{\min} = 1/f_2$ has to be simulated. For the minimal considered (except for $f_2 = 0$) slip frequency of 1 Hz, this leads to a simulation time of $T_{\min} = 1$ s to cover one full magnetization period in the rotor. To prevent subsampling and aliasing of the magnetic flux pulsations in the teeth from slotting harmonics, a sampling frequency of several thousand Hz is necessary. In combination with the simulation time period of $T_{\min} = 1$ s, this would lead to multiple thousand time steps per simulation and thus to an inadequately high computational effort.

To avoid the disadvantage of high computational effort, it is advantageously to shift from time-harmonic iron loss models to those formulated in the time-domain [7,9-13]. In this paper a transient formulation of the iron loss calculation (5) – (9) in the machine is used [9]. In [9] the loss formulation is given in a 3D-Cartesian coordinate system. Since the flux in the stator and rotor core is aligned in radial or tangential direction in most positions, the formulation in polar coordinates is used (6) – (8).

$$p_{\text{hy}}(t) = \rho \cdot \left\{ \left| H_{\text{irr}} \frac{dB_r}{dt} \right| + \left| H_{\text{irr}} \frac{dB_\theta}{dt} \right| \right\} \quad (6)$$

$$p_{\text{cl}}(t) = k_{\text{cl}} \cdot \frac{1}{2\pi^2} \cdot \left\{ \left| \frac{dB_r}{dt} \right|^2 + \left| \frac{dB_\theta}{dt} \right|^2 \right\} \quad (7)$$

$$p_{\text{ex}}(t) = k_{\text{ex}} \cdot \frac{1}{8.763} \cdot \left\{ \left| \frac{dB_r}{dt} \right|^2 + \left| \frac{dB_\theta}{dt} \right|^2 \right\}^{0.75} \quad (8)$$

$$p_{\text{Fe}}(t) = p_{\text{hy}}(t) + p_{\text{cl}}(t) + p_{\text{ex}}(t) \quad (9)$$

In (6), the instantaneous hysteresis loss p_{hy} is given in W/kg and is described by the time differential of the local flux density in radial (B_r) and tangential (B_θ) direction, the irreversible magnetic field strength H_{irr} , and the specific density of the material ρ . Equation (7) describes the Foucault (macroscopic) eddy current loss p_{cl} as time derivative of the magnetic flux density and the material dependent iron loss parameter k_{cl} . Equation (8) determines the excess (microscopic) eddy current losses p_{ex} using the material dependent loss parameter k_{ex} . Equation (9) gives the sum of the three iron loss components as total iron losses $p_{\text{Fe}}(t)$.

In [9], the static hysteresis loop is approximated by an equivalent ellipse. From the ellipse formulation, H_{irr} is modeled by the maximum absolute flux density that is reached in the history of the material B_{max} , the actual absolute value of the flux density B and the hysteresis loss parameter k_{hy} (10). The iron loss parameter k_{cl} is calculated using the material constants, sheet thickness d , specific electrical resistivity ρ_e , and ρ (11) as given in [14].

$$H_{\text{irr}}(B, B_{\text{max}}) = \frac{k_{\text{hy}} \cdot B_{\text{max}}}{\pi \cdot \rho} \cdot \cos \left(\text{asin} \left(\frac{B}{B_{\text{max}}} \right) \right) \\ = \frac{k_{\text{hy}} \cdot B_{\text{max}}}{\pi \cdot \rho} \cdot \sqrt{1 - \left(\frac{B}{B_{\text{max}}} \right)^2} \quad (10)$$

$$k_{\text{cl}} = \frac{\pi^2 d^2}{6 \cdot \rho \cdot \rho_e} \quad (11)$$

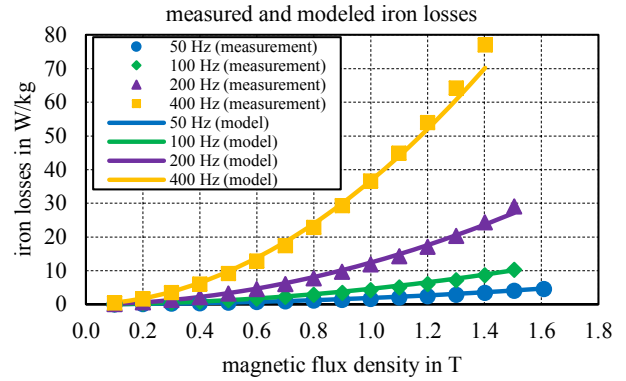


Fig. 9. Measured (ring core) and modeled iron losses for sinusoidal flux density waveform.

parameter	value
k_{hy}	$25.9 \cdot 10^{-3} \text{ W} \cdot \text{kg}^{-1} \cdot \text{s} \cdot \text{T}^{-2}$
k_{cl}	$125.7 \cdot 10^{-6} \text{ W} \cdot \text{kg}^{-1} \cdot \text{s}^2 \cdot \text{T}^{-2}$
k_{ex}	$779 \cdot 10^{-6} \text{ W} \cdot \text{kg}^{-1} \cdot \text{s}^{1.5} \cdot \text{T}^{-1.5}$

In order to find the values of the loss parameters k_{ex} and k_{hy} , ring core measurements of the soft magnetic material are conducted with sinusoidal flux density waveform. The measured ring core has an inner diameter of 100 mm, an outer diameter of 120 mm, a height of 10 mm, and is made of the same material as the magnetic core of the investigated induction machine (M400-50A). Fig. 9 shows the comparison of the measured and modeled iron losses for sinusoidal flux density waveform using the identified iron loss parameter set given in Table I. Comparing measured and modeled iron losses (Fig. 9), a good agreement with a maximum error of 9.6 % at 400 Hz and 1.4 T is apparent. For most of the other points of frequency and magnetic flux density, the difference between modeled and measured iron losses is less than 5 %.

D. Scaling iron losses according to different synchronous frequencies f_1

Due to the fact that the FE simulations are conducted at a single synchronous frequency f_1 , a suitable scaling algorithm for the iron losses at different synchronous frequencies is used. To study the scalability of the iron losses, the cumulated sum of iron losses from $f = 0$ Hz to f_n is used. Equation (12) gives this formulation for the stator Foucault eddy current losses

$$p_{\text{cl},1,\text{sum}}$$

$$p_{cl,1,\text{sum}}(f_n) = \sum_{m=1}^n p_{cl,1}(f_m) \quad (12)$$

$$f_{fp,1} = m_1 \cdot n \cdot N_2 \pm f_1, \quad m_1 = 1, 2, \dots \quad (13)$$

$$f_{fp,2} = m_2 \cdot n \cdot N_1 \pm f_2, \quad m_2 = 1, 2, \dots \quad (14)$$

Besides the fundamental frequency component, flux pulsations occur in the core material. The dependency of the flux pulsating frequencies in the stator $f_{fp,1}$ and in the rotor $f_{fp,2}$ from the mechanical speed n and the stator slot number N_1 and the rotor slot number N_2 are given in (13) and (14).

Fig. 10 and Fig. 11 show the cumulated stator Foucault eddy current losses $p_{cl,1,\text{sum}}$ as defined in (12) as a function of the upper frequency boundary f_n . The operating point in this example is ($I_1 = 202$ A, $f_2 = 5$ Hz). The fundamental frequency of the stator current f_1 is 80 Hz (Fig. 10) and 240 Hz (Fig. 11).

The Foucault stator iron losses that occur at base frequency are 9.2 W ($f_1 = 80$ Hz) and 83.1 W ($f_1 = 240$ Hz). This equals to a factor of 9, which is equal to the square of the increase in frequency f_1 (factor of 3). The mechanical frequency in this example is $n = 37.5$ 1/s and $n = 117.5$ 1/s correspondingly. This leads to flux pulsations in the stator teeth at the frequencies $f_{fp,1} = 970$ Hz and $f_{fp,1} = 1030$ Hz ($f_1 = 80$ Hz, $f_2 = 5$ Hz) and $f_{fp,1} = 3050$ Hz and $f_{fp,1} = 3530$ Hz ($f_1 = 240$ Hz, $f_2 = 5$ Hz). When examining the iron losses in Fig. 10 and Fig. 11, it is found, that the highest share in the overall iron losses is caused by the flux pulsations at $f_{fp,1}(m_1=1)$ (correspondingly for the rotor at $f_{fp,2}(m_2=1)$). Iron losses increase with operation speed. Hence, at high speeds, where the iron losses are dominant, $n \cdot N_1 \gg f_2$ and $n \cdot N_2 \gg f_1$ is assumed. Thus, the iron losses are dominated by losses from flux pulsations. Therefore, the iron losses are scaled according to speed n . Fig. 12 shows the local distribution of the time derivative of the flux density dB/dt . The highest values of $dB/dt > 5000$ T·s⁻¹ are found at the tips of the stator and rotor teeth. Values of $dB/dt > 800$ T·s⁻¹ are found in the stator teeth and yoke. This local distribution illustrates the fact that the largest share of the iron losses is caused by the flux pulsations.

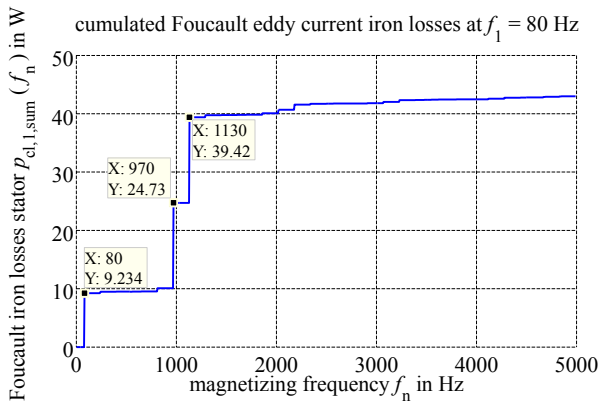


Fig. 10. Simulated cumulated Foucault eddy current iron losses in the frequency domain for the base frequency of $f_1 = 80$ Hz, $f_2 = 5$ Hz, $I_1 = 202$ A.

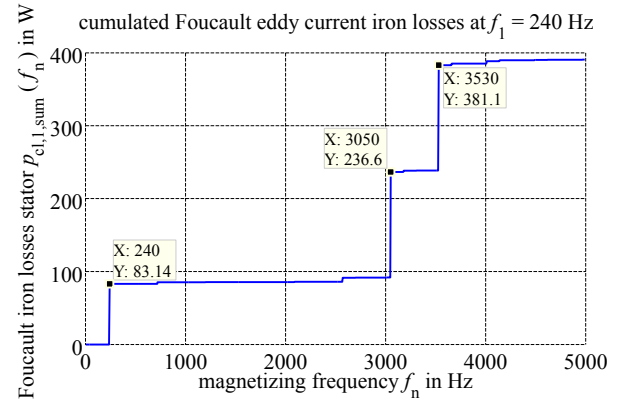


Fig. 11. Simulated cumulated Foucault eddy current iron losses in the frequency domain for the base frequency of $f_1 = 240$ Hz, $f_2 = 5$ Hz, $I_1 = 202$ A.

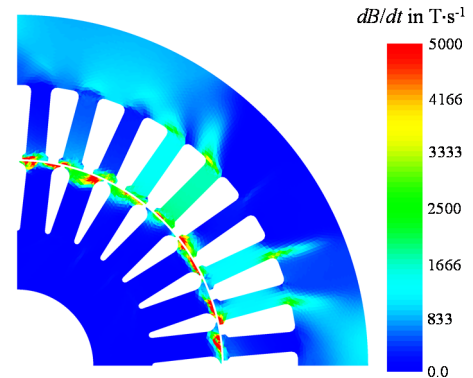


Fig. 12. Simulated time derivative (between two consecutive simulation time steps) of the flux density at $f_1 = 80$ Hz, $f_2 = 5$ Hz, $I_1 = 202$ A.

According to this procedure, the iron loss terms (6) – (8) are evaluated in stator and rotor at one simulation frequency ($f_1 = 80$ Hz) and the loss components are subsequently scaled according to (15) – (17):

$$p_{hy} \propto n \quad (15)$$

$$p_{cl} \propto n^2 \quad (16)$$

$$p_{ex} \propto n^{1.5} \quad (17)$$

The scaling factors (15) – (17) are used to exemplarily scale the losses from $f_1 = 80$ Hz (Fig. 13) to $f_1 = 240$ Hz. An error in the sum of all losses of 1.45 % is found when scaling. The largest relative error of 34.72 % (2.59 W) is made when scaling the rotor hysteresis losses. However, since the hysteresis losses in the rotor are small when compared to the other loss components, the absolute error value of 2.59 W is to be found sufficiently precise. Hence the scaling factors (15) – (17) are applied in the following analysis.

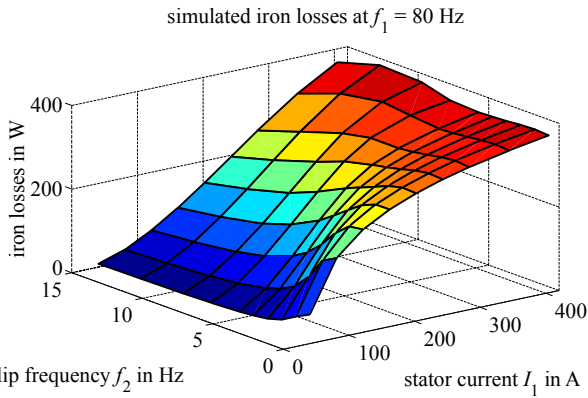


Fig. 13. Simulated iron losses of the machine at a base frequency of 80 Hz.

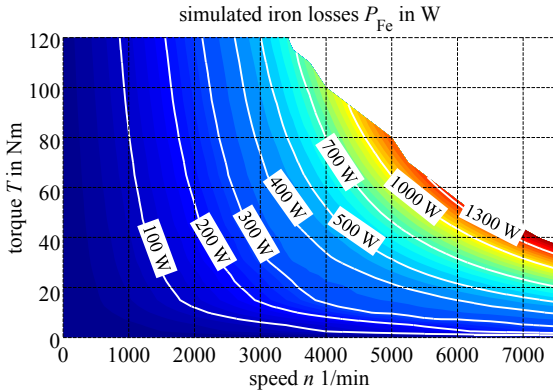


Fig. 14. Simulated machine iron losses.

Fig. 14 shows the simulated iron losses P_{Fe} in terms of torque and speed when choosing the operating points (I_1, f_2) with the lowest possible Ohmic losses for the requested torque T and speed n according to (5).

E. Comparison of measurements and simulations

The operating points from machine measurements are compared to the simulated operating points in terms of torque T , speed n , and total power losses P_{loss} . Fig. 15 shows the test bench for these machine measurements. A Yokogawa® 3000 power analyzer and LEM® IT 400-S current transducers are used to measure the three phase input power P_{3ph} of the machine. A HBM® T12 torque transducer is used to measure torque and speed. From torque and speed, the mechanical power P_{mech} is calculated. The total loss power $P_{loss,meas}$ of the machine is calculated according to (18). The friction losses $P_{friction}$ are measured at different speed values. A quadratic function (19) is fitted to match the measured friction losses.

$$P_{loss,meas} = P_{3ph} - P_{mech} \quad (18)$$

$$P_{friction}(n) = 8.75 \cdot 10^{-3} \text{Ws}^2 \cdot n^2 + 0.375 \text{Ws} \cdot n \quad (19)$$

$$P_{loss,sim} = P_{Cu,1} + P_{Cu,2} + P_{Fe} + P_{friction} \quad (20)$$

Fig. 17 and Fig. 18 show the stator current I_1 and the slip frequency f_2 from measurement and the proposed simulation scheme. The displayed results show a good match between simulated and measured operating behavior in terms of the modelling of the T - n -operating points.

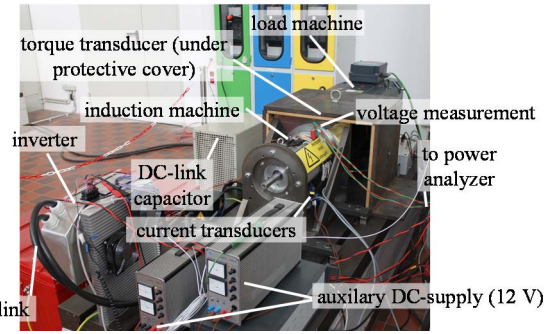


Fig. 15. Machine test bench.

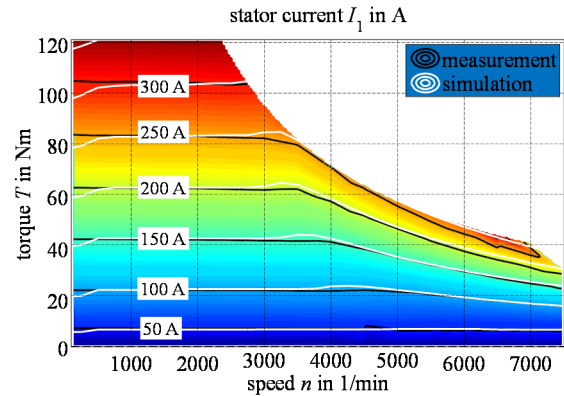


Fig. 16. Comparison of measured and simulated stator current.

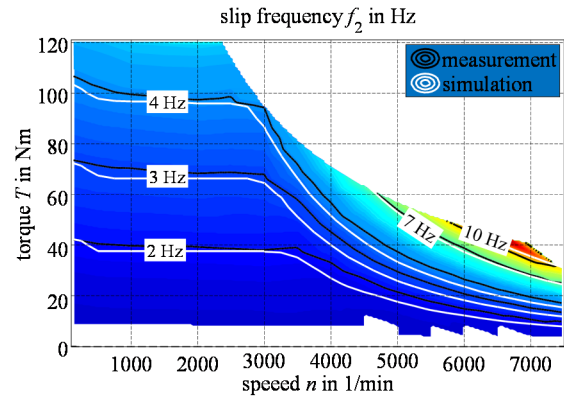


Fig. 17. Comparison of measured and simulated slip frequency f_2 .

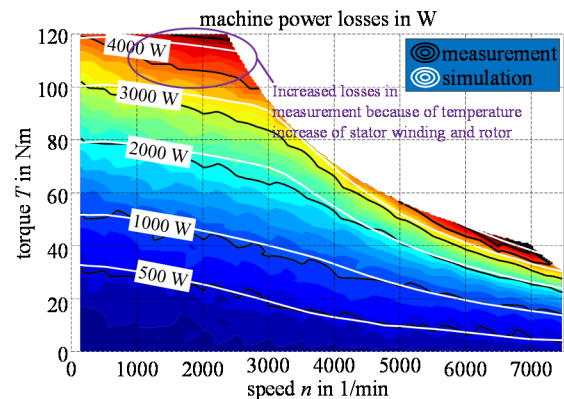


Fig. 18. Comparison of measured and simulated machine power losses P_{loss} .

Fig. 18 shows the comparison of the modeled and measured losses of the machine. At $n = 2500$ 1/min and $T = 120$ Nm the highest deviation for the losses of 700 W (17 %) is found. This deviation is caused by the fact that the stator winding and the rotor heat up quickly at these high load operating points. As a

result, the temperature during the measurement rises and with the temperature the Ohmic resistances in stator and rotor increase which leads to higher Ohmic losses.

III. CONCLUSIONS

The losses of a squirrel cage induction machine operated as traction drive are modeled using a transient iron loss formulation in the post processing of a transient FE simulation at a single synchronous frequency. From the FE simulation, the Ohmic losses in the stator and rotor are calculated at this single synchronous frequency. From the Ohmic losses and the stator flux linkage from the simulation, the operating points in terms of torque and speed are calculated. These operating points were calculated to yield the lowest losses for each point of operation. The limitation of the stator flux linkage due to field weakening operating has been regarded.

A scheme to scale the iron losses from one synchronous frequency to the operating frequency in every operating point of the machine was studied and used. Iron loss measurements of the machines' core material were conducted using a ring core sample of the core material. Iron loss parameters for the iron loss simulation of the machine were extracted from those ring core measurements. The measured friction losses of the machine are added to the modeled losses. A low deviation between the measured and simulated sum of losses was achieved. This loss modelling approach enables for precise machine loss modelling for highly utilized induction machines.

The precise *a-priori* modelling of the machines local losses from FE simulations and ring core measurements enables to predict the influence of changes in the machines' design on the global losses at the design stage. The loss distribution and magnitude is highly depending on harmonics (either from the inverter or the machine itself). For *a-priori* loss modeling, the local and temporal loss distribution is taken into account by transient FE simulation.

The proposed transient approach for operating point dependent loss modeling enables to predict the influence of machine design changes, such as number of poles, electric steel grade, diameters, length, and many other design factors, along the whole torque-speed map.

IV. REFERENCES

[1] Kusko, A.; Galler, D., "Control Means for Minimization of Losses in AC and DC Motor Drives," in *Industry Applications, IEEE Transactions on*, vol. IA-19, no.4, pp.561-570, July 1983.

[2] Garcia, G.O.; Mendes Luis, J.C.; Stephan, R.M.; Watanabe, E.H., "An efficient controller for an adjustable speed induction motor drive," in *Industrial Electronics, IEEE Transactions on*, vol.41, no.5, pp.533-539, Oct 1994.

[3] Zengcai Qu; Ranta, M.; Hinkkanen, M.; Luomi, J., "Loss-minimizing flux level control of induction motor drives," in *Electric Machines & Drives Conference (IEMDC), 2011 IEEE International*, vol., no., pp.1585-1590, 15-18 May 2011.

[4] Odhano, S.A.; Bojoi, R.; Boglietti, A.; Rosu, S.G.; Griva, G., "Maximum Efficiency per Torque Direct Flux Vector Control of Induction Motor Drives," in *Industry Applications, IEEE Transactions on*, vol.51, no.6, pp.4415-4424, Nov.-Dec. 2015.

[5] Sridharan, S.; Krein, P.T., "Induction motor drive design for traction application based on drive-cycle energy minimization," in *Applied Power Electronics Conference and Exposition (APEC), 2014 Twenty-Ninth Annual IEEE*, vol., no., pp.1517-1521, 16-20 March 2014.

[6] Windisch, T.; Hofmann, W., "Loss minimizing and saturation dependent control of induction machines in vehicle applications," in *Industrial Electronics Society, IECON 2015 - 41st Annual Conference of the IEEE*, pp.001530-001535, 9-12 Nov. 2015.

[7] Kowal, D.; Sergeant, P.; Dupre, L.; Karmaker, H., "Comparison of Frequency and Time-Domain Iron and Magnet Loss Modeling Including PWM Harmonics in a PMSG for a Wind Energy Application," in *Energy Conversion, IEEE Transactions on*, vol.30, no.2, pp.476-486, June 2015.

[8] Ruf, A.; Thul A.; Steentjes, S.; Hameyer, K., "Loss minimizing control strategy for electrical machines considering iron loss distribution," in *2015 IEEE International Electric Machines & Drives Conference (IEMDC)*, pp. 974-980, 10-13 May 2015.

[9] Lin, D.; Zhou, P.; Fu, W.N.; Badics, Z.; Cendes, Z.J., "A dynamic core loss model for soft ferromagnetic and power ferrite materials in transient finite element analysis," in *Magnetics, IEEE Transactions on*, vol.40, no.2, pp.1318-1321, March 2004.

[10] Belahcen, A.; Arkkio, A., "Comprehensive Dynamic Loss Model of Electrical Steel Applied to FE Simulation of Electrical Machines," in *Magnetics, IEEE Transactions on*, vol.44, no.6, pp.886-889, June 2008.

[11] Rasilo, P.; Dlala, E.; Fonteyn, K.; Pippuri, J.; Belahcen, A.; Arkkio, A., "Model of laminated ferromagnetic cores for loss prediction in electrical machines," in *Electric Power Applications, IET*, vol.5, no.7, pp.580-588, August 2011.

[12] Hafner, M.; Henrotte, F.; Herranz Gracia, M.; Hameyer, K., "An Energy-Based Harmonic Constitutive Law for Magnetic Cores With Hysteresis," in *Magnetics, IEEE Transactions on*, vol.44, no.6, pp.922-925, June 2008.

[13] Dlala, E.; Bottauscio, O.; Chiampi, M.; Zucca, M.; Belahcen, A.; Arkkio, A., "Numerical Investigation of the Effects of Loading and Slot Harmonics on the Core Losses of Induction Machines," in *Magnetics, IEEE Transactions on*, vol.48, no.2, pp.1063-1066, Feb. 2012.

[14] Lammeraner, J.; Staffl M., "Eddy Currents," Iliffe Books Ltd., London, 1966.

V. BIOGRAPHIES

Georg von Pfingsten received his Bachelor's degree in October 2010 and his Master's degree in November 2012 in electrical engineering from RWTH Aachen University, Germany.

He has been working as a research associate at the Institute of Electrical Machines since December 2012. His research interests include induction machine modelling, optimization of induction machines, soft magnetic material modelling, and iron loss calculation in macroscopic scale.

Simon Steentjes received the Diploma degree in electrical engineering from RWTH Aachen University, Germany, in November 2011.

He has been working as a research associate at the Institute of Electrical Machines since December 2011. His research interests include hard- and soft magnetic material modelling on the micro- and macroscopic scale, iron loss calculation, effects of material processing, magnetic forces, and mathematical methods.

Dr. Kay Hameyer is full professor and the director of the Institute of Electrical Machines (IEM) at RWTH Aachen University in Germany. His research interests are numerical field computation and optimization, the design and controls of electrical machines. Dr. Hameyer is author of more than 250 journal publications, more than 500 international conference publications, and author of 4 books. Dr. Hameyer is a member of VDE, IEEE senior member, fellow of the IET.